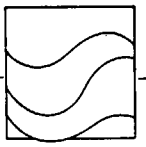

South Equatorial Countercurrent
South Equatorial Undercurrent
South Atlantic Ocean

Contre-Courant Équatorial Sud
Sous-Courant Équatorial Sud
Océan Atlantique Sud

Observations in the subthermocline undercurrent of the Equatorial South Atlantic Ocean : 1978-1980

R. L. Molinari[a], B. Voituriez[b], P. Duncan[c]

[a] National Oceanic and Atmospheric Administration, Atlantic Oceanographic and Meteorological Laboratories, Miami, Florida 33149, USA.

[b] Office de la Recherche Scientifique et Technique Outre-Mer, Centre Océanologique de Bretagne, BP n° 337, 29273 Brest Cedex, France.

[c] University of California, Lawrence Berkeley Laboratory, Berkeley, California, USA.

Received 16/3/81, in revised form 18/5/81, accepted 23/5/81.

ABSTRACT

Observations collected prior to, during, and after the Global Weather Experiment in the region of the subthermocline undercurrent in the South Atlantic, referred to here as the South Equatorial Undercurrent (SEUC), are presented. Four cruises to the western Atlantic and two at 4°W provide data on the current, temperature, salinity, oxygen and silicate structure of the SEUC. The core of the SEUC is typically located between 3°S and 5°S with a width of about 100 km and a core depth between 150 and 200 m. In the western Atlantic, the average transport of the SEUC has a mean of $15 \times 10^6 m^3/sec$. Variability about the mean is related to recirculation in eddy-like features of water along the edge of the SEUC which do not contribute to the net eastward transport. Water mass property distributions within the SEUC are similar to those observed previously. For instance, the SEUC represents the southern boundary of the equatorial thermostad and halostad. The core of the SEUC is associated with a relative maxima in oxygen distribution.

Oceanol. Acta, 1981, **4**, 4, 451-456.

RÉSUMÉ

Observations, sous la thermocline, du Contre-Courant Équatorial Sud de l'Atlantique en 1978-1980.

Le Contre-Courant Équatorial Sud de l'Atlantique qui coule sous la thermocline, et que l'on appelle ici Sous-Courant Équatorial Sud, est étudié à partir des observations faites avant, pendant et après l'Expérience Météorologique Mondiale du GARP. Les données utilisées pour décrire sa structure : vitesse, température, salinité, oxygène et silicates, proviennent de quatre campagnes faites dans l'ouest de l'Atlantique et de deux campagnes, le long de 4°W. Le noyau du Sous-Courant Équatorial Sud se situe entre 150 et 200 m de profondeur et il a une largeur de 100 km. Dans l'ouest de l'Atlantique, le transport est en moyenne de $15.10^6 m^3.s^{-1}$. La variabilité du transport est liée à des structures quasi tourbillonnaires qui se produisent sur les bords et ne contribuent pas au transport net vers l'Est. Les propriétés des eaux du Sous-Courant Équatorial Sud sont semblables à celles déjà observées auparavant : elles constituent la limite sud de ce que l'on appelle la thermostad et la halostad équatoriales. Elles sont associées à un maximum d'oxygène.

Oceanol. Acta, 1981, **4**, 4, 451-456.

INTRODUCTION

Observations in the equatorial Atlantic Ocean (Khanaychenko, Khlystov, 1966; Mazeika, 1968; Hisard *et al.*, 1976; Cochrane *et al.*, 1979; and Bubnov, Egorikhin, 1980) and the equatorial Pacific Ocean (Tsuchiya, 1975) reveal the presence in each ocean of three subsurface currents flowing to the East. Typically, the cores of the three undercurrents are located between 5°S and 5°N.

The Equatorial Undercurrent (EUC) is located on the equator, within the thermocline. Subthermocline undercurrents are located in both hemispheres at approximately equal distances from the equator. As demonstrated by Tsuchiya (1975), Hisard *et al.* (1976) and Cochrane *et al.* (1979), the undercurrents are distinct from the primarily surface North Equatorial Countercurrent (NECC) and South Equatorial Countercurrent (SECC) observed in both oceans. To distinguish the undercurrents from the SECC and NECC, hereinafter, the tropical South Atlantic undercurrent will be referred to as the South Equatorial Undercurrent (SEUC) and its northern hemisphere counterpart as the North Equatorial Undercurrent (NEUC) [as first suggested by Tsuchiya (1975) for the Pacific undercurrent].

The SEUC has been traced across the South Atlantic, from origins off the coast of Brazil (Cochrane *et al.*, 1979) to at least 5°W in the Gulf of Guinea (Hisard *et al.*, 1976). Cochrane *et al.* (1979) determined an average geostrophic transport for the SEUC from four sections of 15 Sv (1 Sv = 10^6 m^3/sec.). Individual transport values ranged from 13 Sv to 20 Sv. More data were available in the NEUC between 40°W and 28°W, here transports ranged from 13 Sv to 40 Sv.

Data collected prior to, during, and after the Global Weather Experiment, in both the western and eastern Atlantic, reveal that considerable spatial and temporal variablity exist in the properties of the SEUC. In the following sections, data collection techniques are described, directly measured and geostrophic speed sections through the SEUC are given, transports are computed and temperature, salinity, and nutrient sections are described. Dynamic height distributions show the cause of some of the variability in SEUC transport.

OBSERVATIONS

Data were collected between 25 and 29°W from the NOAA Ship Researcher of the United States of America and along 4°W during August 1978 and April 1979 from the ORSTOM Ship Capricorne of France. Conductivity temperature depth (CTD) units, expendable bathythermograph (XBT) probes, profiling current meter (PCM) units, and water sample bottles were used. Table 1 shows the time of the cruises and the sensors used to define the characteristics of the SEUC.

CTD calibration data were collected on both vessels from water sample bottles which provide temperature and salinity data. In addition, oxygen and nutrient samples were drawn from these bottles on several cruises. The calibrated data are accurate to within $\pm .01$°C in temperature and $\pm .01^0/_{00}$ in salinity. Assuming no navigational errors, maximum errors induced in geostrophic computations by these accuracies are of the order of 5 cm/sec. in the sampling area. Navigation errors induce an error in the geostrophic computations of the order of 3% of the speed.

Table 1

Sensors used to describe the SEUC characteristics.

Month/Year	Ship	CTD	PCM	XBT
July-August 1978	Researcher	X	X	X
August 1978	Capricorne	X		
January-February 1979	Researcher	X		X
April 1979	Capricorne	X		
July 1979	Researcher		X	X
February-March 1980	Researcher	X	X	X

The PCM provides vertical profiles of horizontal velocity relative to ship's drift (*see* Duing, Johnson, 1972, for a description of the instrument). Absolute velocity profiles can be obtained only after the ship's drift is removed from the PCM profile. Standard navigational techniques (Omega, satellite) are inadequate in equatorial areas to define ship drift accurately during the PCM cast. The PCM casts were to a maximum depth of either 500 or 600 m. In view of the absence of reliable ship's drift data, observed currents were referenced to these levels. The relative PCM speed components are probably accurate to within ± 10 cm/sec.

GEOSTROPHIC AND DIRECTLY MEASURED SPEED SECTIONS AND TRANSPORTS

Geostrophic speed sections are given in Figures 1 and 2.

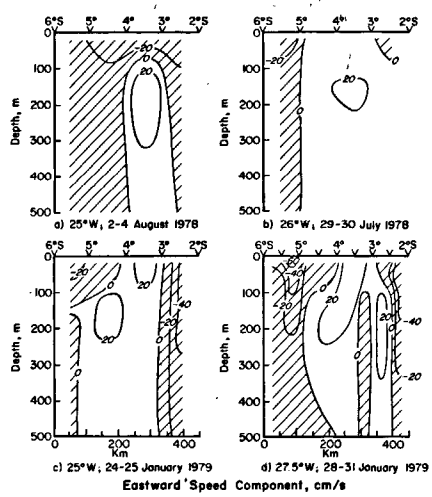

Figure 1

Vertical sections of geostrophic current speed computed relative to 1 000 db for the time periods indicated. Shaded areas indicate flow to the west; tick marks indicate station positions.

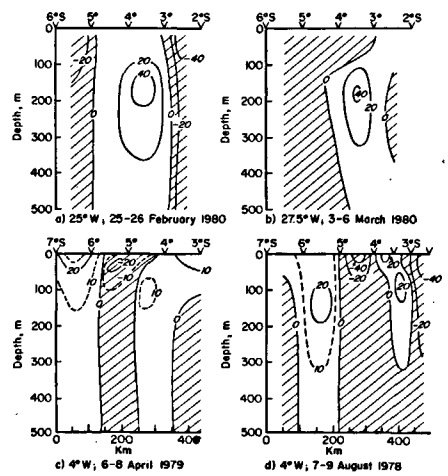

Figure 2

Same as Figure 1.

The geostrophic computations are made relative to a reference level of 1 000 m. Geostrophic speeds at 500 and 600 m, the reference level for PCM stations, are generally less than 10 cm/sec.

The core of the SEUC will be taken here as the flow within the 20 cm/sec. isotach, in view of the PCM accuracy and for comparison with other observations of the equatorial undercurrents. In the western Atlantic, typically, a single SEUC core is observed between 3°S and 5°S. However, two cores are observed along 27.5°W during January 1979 (Fig. 1 *d*). A double core is also observed at 4°W during August 1978 (Fig. 2 *d*). A surface countercurrent is observed between 6°S and 7°S during April 1979 (Fig. 2 *c*). Cochrane *et al.* (1979) describe similar multiple cores for both the NEUC and SEUC east of about 30°W.

In the vertical, the SEUC core (again using the 20 cm/sec. isotach) extends from a minimum depth of about 100 m to maximum depths ranging from 200 m (Fig. 1 *b*) to greater than 300 m (Fig. 2 *a*). In both the eastern and western Atlantic, the core of the SEUC is about 120 km wide. Maximum geostrophic speeds in the core of the SEUC range from 20 cm/sec. in the eastern Atlantic (Fig. 2 *d*) to 40 cm/sec. in the western Atlantic (Fig. 2 *a* and 2 *b*).

In the western Atlantic, geostrophic computations are possible for two southern hemisphere winter periods and for one summer period (Fig. 1 and 2). No systematic seasonal differences are apparent. Largest differences between sections occur within synoptic observing periods. For instance, during July 1978 (Fig. 1 *a* and 1 *b*), eastward flow extends to at least 4.5°S at 26°W, but not at 25°W. Eastward geostrophic flow extends vertically from the SEUC core to the sea surface at 25°W, but not at 26°W during July 1978 (Fig. 1 *a* and 1 *b*). Similar zonal differences in the current structure are observed during March 1980 (Fig. 2 *a* and 2 *b*).

PCM zonal speed sections at 25°W (Fig. 3) give somewhat different current distributions than do the concurrent geostrophic speed sections (Fig. 1 and 2). These differences are caused by the different characteristics of each sampling scheme. The PCM samples velocities at a point, while a geostrophic observation represents the average speed over the distance between CTD stations. Thus, a PCM profile in the core of the SEUC as during August 1978 at 25°W (Fig. 3 *a*), would, depending on CTD station spacing and zonal slopes, typically give higher speeds than would CTD stations which bracket the core (Fig. 1 *a*). If the PCM were not taken in the core, the geostrophic speed could be higher, which may be the case during February 1980 (Fig. 2 *a* and 3 *c*).

The width of the core of the SEUC, again given by the 20 cm/sec. isotach, is similar on both the geostrophic and PCM sections. However, the core of the SEUC is consistently deeper on the PCM sections. The position of the SEUC relative to the EUC is apparent on the PCM sections. The two eastward flows typically are separated by westward flows.

Geostrophic and directly measured transports are computed from CTD and PCM using two definitions for the transport of the SEUC. Cochrane *et al.* (1979) define the SEUC as that flow bounded by a ridge and trough in the equatorial dynamic height field and the 200 cl/t and 80 cl/t isanosteres. The PCM stations, however, do not reach the depth of the 80 cl/t isanostere (800-900 m). Therefore, because of the accuracy of the PCM measurements (previously described), directly measured transports are computed for the flow within the 20 cm/sec. isotach. Table 2 lists transports computed geostrophically using the definition of Cochrane *et al.* (1979) and the 20 cm/sec. isotach as limits. Differences in the transport values calculated geostrophically and direct measurements at the same section, as in the case of speeds, can be attributed to differences in sampling technology.

Considerable variability is observed in the SEUC transports. No apparent seasonal signal is obvious, with the largest variability observed during synoptic cruise intervals (e.g., July-August 1978, February-March 1980). Cochrane *et al.* (1979) computed an average

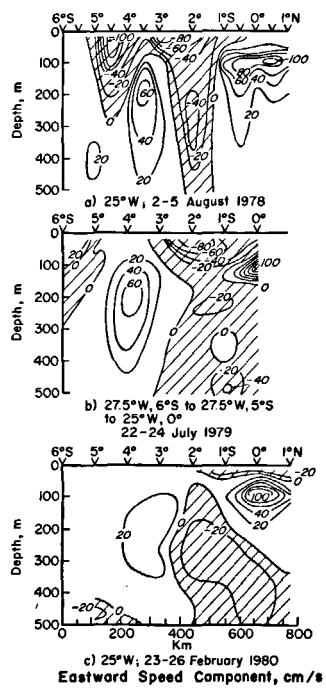

Figure 3

Directly measured sections of zonal speed relative to 500 *m, a, and* 600 *m, 3 b and 3 c. Shaded areas indicate flow to the west; tick marks indicate station positions.*

Table 2

Transports of the South Equatorial Undercurrent in Sverdrups (10^6 m^3/*sec.*).

Month/ Year	Longitude °W	Geostrophic (*)	Within 20 cm/sec. Geostrophic	Isotach Direct
3/63 (**)	33°	15.9		
3/63 (**)	30°	20.1		
2/63 (**)	25°	13.1		
8/63 (**)	25°	13.0		
7/78	26°	20.0	2.2	
8/78	25°	9.7	6.8	
2/79	27.5°	10.7	5.5	
2/79	25°	11.4	3.4	
7/79	27.5°-25° (***)			19.1
3/80	27.5°	7.4	8.1	3.3
2/80	25°	28.3	10.9	11.9

(*) Computed relative to 1 000 m between the 80 cl/t and 200 cl/t isanosteres and the equatorial ridge and trough. (**) From Cochrane *et al.* (1979). (***) Section occupied from 6°S, 27.5°W to 5°S, 27.5°W to 0°, 25°W.

transport of 15 Sv from the four 1963 sections given on Table 2. The average transport computed using their definition and all the data of Table 2 is also 15 Sv. However, the range of SEUC transport values, 10 Sv to 28 Sv, is similar to the range found from the NEUC by Cochrane *et al.* (1979).

TEMPERATURE, SALINITY, AND NUTRIENT SECTIONS

Temperature and salinity sections derived from data collected along 25°W during February 1980 and along 4°W during April 1979 reveal many of the properties of the temperature and salinity distributions of the SEUC. The 25°W temperature and salinity sections are given on Figure 4 and the 4°W sections on Figure 5. The 20 cm/sec. isotach representing the core of the SEUC from the appropriate geostrophic speed section also is shown on these figures.

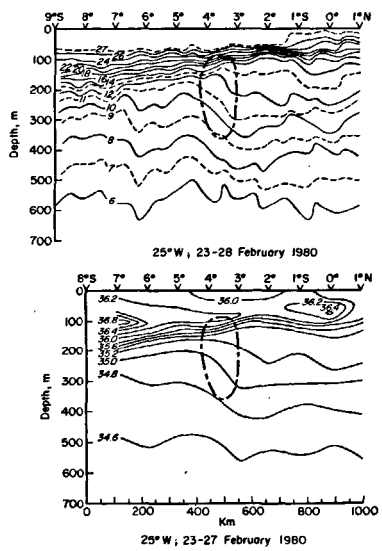

Figure 4

Temperature section (upper panel) and salinity section (lower panel) along 25°W observed during February 1980. Tick marks indicate station positions. XBT data are also included in the temperature section. The 20 cm/sec. isotach representing the core of the SEUC for the same time period is also shown.

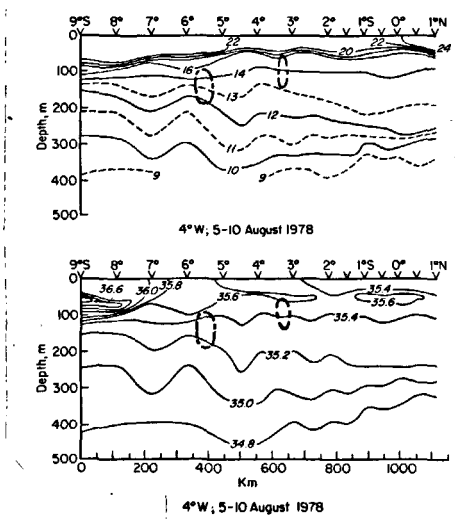

Figure 5

Same as Figure 4, except for 4°W observed during August 1978.

The temperature and salinity distributions on Figures 4 and 5 are very similar to distributions observed by other investigators (Hisard *et al.*, 1976; Gate Atlas, 1980, for instance). The core of the SEUC at both 4°W and 25°W coincides with the equatorward increase in depth of the isotherms between 8 and 13°C. This increase in depth is typically observed between 3°S and 5°S, at 25°W (Fig. 4). The thickness of the layer bounded by the 12°C and 14°C isotherms also increases at these latitudes. Reduced vertical temperature gradients are associated with this portion of the water column frequently called the thermostad. The thermostad is continuous across the equator and into the northern hemisphere, where temperature and current patterns are the mirror images of those observed in Figure 4; that is, these isotherms rise to the north in the vicinity of the NEUC (Philander, Duing, 1980, for instance).

Temperature sections at 25°W for other time periods (not shown) reveal variability in the position of maximum isotherm slopes, in the value of maximum slopes and in the total depth range of the 10 to 14°C isotherms. However, no apparent seasonal signal is visible in this variability. There are systematic differences between the temperature structure at 25°W and at 4°W. In particular, the 10°C isotherm at 4°W is at greater depths than at 25°W at latitudes south of 5°S, but at comparable depths north of 5°S, indicating less depth range in the isotherms at these depths. Furthermore, there is some suggestion that the thermostad occurs at higher temperatures at 4°W (the 14°C isotherm is apparently within the thermostad during April 1979, Fig. 5).

Cochrane *et al.* (1979) find that the flux mode of the SEUC lies between the 120 and 140 cl/t isanosteric surfaces. In the equatorial Atlantic, these surfaces are within the thermostad. A similar flux mode was computed from the transport data of Table 2. Mean temperatures and transports for this portion of the water column are given on Table 3. The temperature at this level increases to the east during August 1978 at the rate of 2.6×10^{-5}°C/m between 25°W and 4°W. The thermostad underneath the EUC warmed between 33°W and 10°W during the summer of 1974 at the rate of 4.4×10^{-5}°C/m (Katz *et al.*, 1979).

No extrema in salinity are coincident with the core of the SEUC (Fig. 4 and 5). In the region of the SEUC, isohalines exhibit properties similar to those of the isotherms. At 25°W, isohalines from $34.6^0/_{00}$ to

Table 3

Geostrophic transport computed relative to 1000 m and average temperature between the 120 cl/t and 140 cl/t isanosteric surfaces.

Month/Year	Latitude (°W)	Transport (Sv)	Temperature (°C)
08/78	26°	9.3	10.9
08/78	25°	3.5	10.6
08/78	4°	N.A.	11.6
02/79	27.5°	5.1	11.1
02/79	25°	3.5	11.0
04/79	4°	N.A.	11.7
03/80	27.5°	5.2	11.0
03/80	25°	15.6	10.9

$35.2^0/_{00}$ sink towards the equator (Fig. 4), with maximum slopes coincident with maximum isotherm slopes. A halostad, bounded by the 35.0 and $35.4^0/_{00}$ isohalines (Fig. 4), forms coincidentally with the thermostad. As in the case of the temperature structure, no significant seasonal variability is apparent in the salinity structure. Again, as in the case of the temperature structure, downstream changes in the salinity structure are observed. For instance, the halostad appears saltier to the east, as observed under the EUC by Katz *et al.* (1979). Also, the $35.0^0/_{00}$ isohaline has less vertical depth range at 4°W than at 25°W (Fig. 4 and 5), as do the isotherms at these depths.

Oxygen and silicate sections obtained during February-March 1980 are given on Figures 6 and 7. The core of the SEUC is coincident with a region both in the vertical and meridionally of relatively high oxygen concentration embedded within a large-scale oxygen minimum layer (Fig. 6). Similar relations between the SEUC core and oxygen distribution have been observed previously (Equalant Atlas, 1973; Hisard *et al.*, 1976). The core of the SEUC does not appear associated with any clearcut minima or maxima in silicate distribution (Fig. 7) or phosphate distribution (not shown). However, there is some suggestion of a slight minimum in silicate concentration (as indicated by a spreading of the silicate concentration isolines) to the north of the SEUC core.

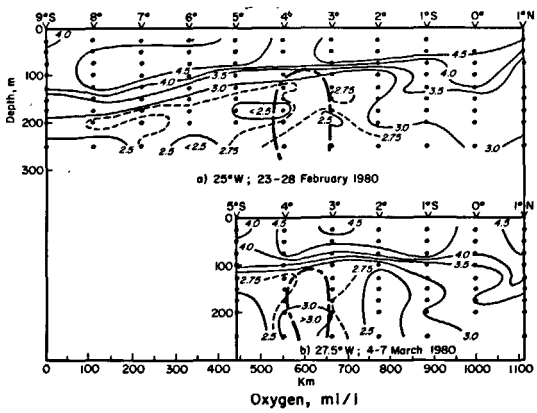

Figure 6

Oxygen concentration sections along 25°W and 27.5°W obtained during February-March 1980. Tick marks indicate station positions. The 20 cm/sec. isotach representing the core of the SEUC for the appropriate section is also shown.

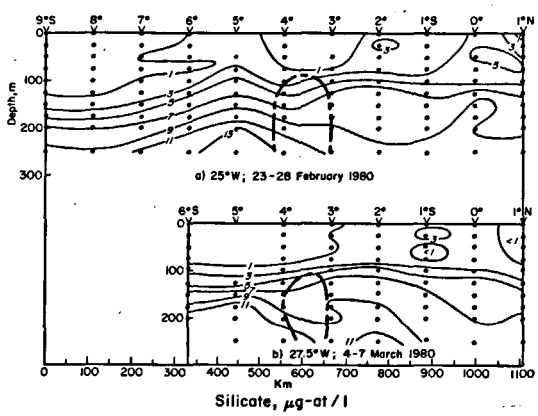

Figure 7

Same as Figure 6, except for silicate concentration.

DISCUSSION

The core of the SEUC is typically observed at 200 db (Fig. 1, 2, and 3). Thus, dynamic topography distributions at this level will reveal the horizontal distributions of currents at the core layer of the SEUC. As in the case of the NEUC (Cochrane *et al.*, 1979), considerable variability in the zonal direction is observed in the intensity of the equatorial ridges and troughs. The variability appears as closed circulation features along the edges of the SEUC (Fig. 8) which implies that much of the transport variability is caused by recirculation around these small-scale features. For instance, the geostrophic transport of the SEUC during July-August 1978 was 20.0 Sv at 26°W and 9.7 Sv at 25°W. The dynamic topography for this period (Fig. 8) shows that a closed clockwise gyre exists at 27-26°W to the south of the SEUC and a counterclockwise gyre exists to the north at these latitudes. The larger transport at 26°W is caused by recirculation around these features and does not represent the net eastward transport of the SEUC.

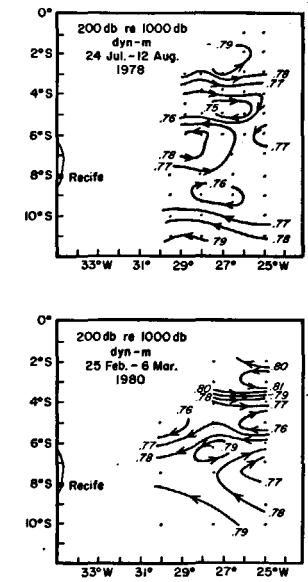

Figure 8

Distribution of the dynamic topography of the 200 db surface computed relative to 1 000 db for the time periods indicated.

Tsuchiya (1975) reported considerable variability in the geostrophic transports of the Pacific NEUC and SEUC on short space scales. For instance, during February 1967, SEUC transport at 119°W was 3 Sv, while at 98°W, the transport was 6 Sv. The distribution of the depth of the 160 cl/t isanostere (Fig. 10-δ 160-z, Love, 1972) suggests the difference in transport is related to closed circulation features along the edge of the SEUC, as is the case in the Atlantic.

Further analysis is required to determine the cause of the circulation features along the edges of the NEUC and SEUC. In particular, it is unknown if these subsurface features are related to surface phenomena such as waves observed within the South Equatorial Current (Legeckis, 1977).

The property distributions described earlier are consistent with the contention of Cochrane *et al.* (1979) that the SEUC begins at about 5°S off the Brazilian coast. In particular, the oxygen section on Figure 6 reveals that the core of the SEUC is coincident with a maximum in

oxygen distribution. Oxygen distributions at 150 m given in the Equalant Atlas (1973) show tongues of high oxygen originating off the Brazilian coast and extending east along the axis of the SEUC during the two 1963 Equalant studies. Hisard *et al.* (1976) trace this high oxygen core at least to 5°W. No salinity extrema are associated with the core of the SEUC on Figures 4 and 5. Similarily, no extrema are observed on the 150 m salinity distributions given in the Equalant Atlas (1973).

As in the case of the Pacific undercurrents (Bruce Taft, pers. comm.), water mass properties should be a useful tool in delineating the *net* flow of the Atlantic subsurface flows. For instance, if data with sufficient spatial resolution existed, the oxygen signal of the Atlantic SEUC could be used to mark the boundaries of the SEUC. This would eliminate the transport added by the features which recirculate the water along the edges of the flow. Unfortunately, the spatial resolution during the cruises presented is inadequate to perform this computation. Using property distributions instead of pressure gradient distributions to mark the boundaries of the undercurrents, much of the transport variability described by Tsuchiya (1975), Cochrane *et al* (1979), and in this paper might be reduced.

The equatorial undercurrents and interleaving westward flows probably play an important role in transporting water mass properties across the equatorial oceans. For instance, dramatic seasonal (upwelling in the Gulf of Guinea) and interannual (El Niño) differences in thermal properties of the eastern equatorial oceans have been observed. In the case of the Pacific Ocean, Wyrtki (1975) hypothesizes that the NECC and SECC may contribute to the occurrence of El Niño through increased transport of heat from west to east. The possible role of the NEUC and SEUC in El Niño event has not yet been considered.

Some suggestion of interaction between the undercurrents and associated thermal fields is found in the eastward warming of the thermostad in both the Atlantic and Pacific (Tsuchiya, 1975). Katz *et al.* (1979) hypothesize that the thermostad below the EUC is warmed through diffusion of heat from the EUC to the thermostad. Since the SEUC is observed within the southern boundary of the thermostad, this mechanism is not operative. An alternative explanation has not yet been offered.

Acknowledgements

This effort was partially funded by the Department of Energy through agreements with the Lawrence Berkeley Laboratory of the University of California and the Atlantic Oceanographic and Meteorological Laboratories (AOML) of the National Oceanic and Atmospheric Administration and was a contribution of the French Program "Ciprea". Additional funding was provided to AOML by the NOAA Special Research Programs Office. The contributions of the officers and crews of the Researcher and Capricorne in obtaining these data were invaluable. The valuable suggestions of Drs. Eli Katz and M. Tsuchiya are also gratefully acknowledged.

REFERENCES

Bubnov V. A., Egorikhin V. D., 1980. Study of water circulation in the tropical Atlantic, *Deep-Sea Res.*, **26**, Suppl. 2, 125-136.

Cochrane J. D., Kelly F. J., Olling C. R., 1979. Subthermocline countercurrents in the western equatorial Atlantic Ocean, *J. Phys. Oceanogr.*, **9**, 724-738.

Duing W., Johnson D. R., 1972. High resolution current profiling in the Straits of Florida, *Deep-Sea Res.*, **19**, 259-274.

Equalant Atlas, 1973. *Equalant I and Equalant II oceanographic atlas*, Vol. **1** and **2**, edited by Kolesnikov, UNESCO, Paris.

Gate Atlas, 1980. *Physical oceanography of the tropical Atlantic during Gate*, edited by W. Duing, F. Ostapoff and J. Merle, Univ. Miami, Miami, Florida.

Hisard P., Citeau J., Morlière A., 1976. Le système des contre-courants équatoriaux subsuperficiels, permanence et extension de la branche sud dans l'Océan Atlantique, *Cah. ORSTOM, sér. Oceanogr.*, **14**, 209-220.

Katz E. J., Bruce J. G., Petrie B. D., 1979. Salt and mass flux in the Atlantic Equatorial Undercurrent, *Deep-Sea Res.*, **26**, Suppl. 2, 137-160.

Khanaychenko N. K., Khlystov N. Z., 1966. The south branch of the equatorial countercurrent in the Atlantic Ocean, *Dokl. USSR Akad. Sci.*, **166**, 205-207.

Legeckis R., 1977. Long waves in the eastern equatorial Pacific Ocean: a view from a geostationary satellite, *Science*, **197**, 1179-1181.

Love C. M., editor, 1972. *Eastropac Atlas*, vol. **1**, Circ. 330, National Marine Fisheries Service, Washington, DC.

Mazeika P. A., 1968. Eastward flow within the South Equatorial Current in the eastern south Atlantic, *J. Geophys. Res.*, **73**, 5819-5828.

Philander G., Duing W., 1980. The oceanic circulation of the tropical Atlantic, and its variability, as observed during Gate, *Deep-Sea Res.*, **26**, Suppl. 2, 1-27.

Tsuchiya M., 1975. Subsurface countercurrents in the eastern equatorial Pacific Ocean, *J. Mar. Res., Suppl.*, **23**, 145-175.

Wyrtki K., 1975. El Niño, the dynamic response of the equatorial Pacific Ocean to atmospheric forcing, *J. Phys. Oceanogr.*, **5**, 572-584.